BRNO UNIVERSITY OF TECHNOLOGY

VYSOKÉ UČENÍ TECHNICKÉ V BRNĚ

FACULTY OF MECHANICAL ENGINEERING

FAKULTA STROJNÍHO INŽENÝRSTVÍ

INSTITUTE OF AEROSPACE ENGINEERING

LETECKÝ ÚSTAV

AERODYNAMIC DESIGN OF RACING CAR ENGINE AIR INTAKE

AERODYNAMICKÝ NÁVRH VSTUPU VZDUCHU MOTORU SPORTOVNÍHO VOZU

BACHELOR'S THESIS

BAKALÁŘSKÁ PRÁCE

AUTHOR **Jáchym Galáš**

AUTOR PRÁCE

SUPERVISOR **Ing. Robert Popela, Ph.D.**

VEDOUCÍ PRÁCE

BRNO 2024

BRNO UNIVERSITY OF TECHNOLOGY FACULTY OF MECHANICAL ENGINEERING

Assignment Bachelor's Thesis

Institut:	Institute of Aerospace Engineering
Student:	**Jáchym Galáš**
Degree programm:	Fundamentals of Mechanical Engineering
Branch:	no specialisation
Supervisor:	**Ing. Robert Popela, Ph.D.**
Academic year:	2023/24

As provided for by the Act No. 111/98 Coll. on higher education institutions and the BUT Study and Examination Regulations, the director of the Institute hereby assigns the following topic of Bachelor's Thesis:

Aerodynamic design of racing car engine air intake

Brief Description:

Race car engine performance is directly affected by pressure losses and distorsion of flowfield in air intake system. Major parameters having influence on intake quality are position of intake on car body, shape of channel and its dimensions.

Bachelor's Thesis goals:

Analysis of possible installation and shape of air intake for race car engine.

Recommended bibliography:

Constandi, J., S., Air Induction Design for Restricted Race Engines, https://core.ac.uk/download/pdf/37749992.pdf.

Katz, J., Race Car Aerodynamics: Designing for Speed, Bentley Publishers, ISBN 0837601428.

Deadline for submission Bachelor's Thesis is given by the Schedule of the Academic year2023/24

In Brno,

L. S.

doc. Ing. Jaroslav Juračka, Ph.D. Director of the Institute	doc. Ing. Jiří Hlinka, Ph.D. FME dean

ABSTRACT

This study employs computational fluid dynamics (CFD) to compare the aerodynamic performance of two distinct designs for race car and sports car engine air inlets: a NACA-style submerged inlet and a roof scoop. These designs represent two prevalent approaches in race car and sports car aerodynamics, each offering unique advantages and challenges. For an engine, one of the key factors in its performance is the pressure under which the air is delivered into the combustion chamber. For this reason, it is important to design the inlet so that the pressure losses are as low as possible. The results provide a better understanding of the two design philosophies which are then compared and possible improvements and solutions for further iterations are proposed.

KEYWORDS

Aerodynamics, Computational Fluid Dynamics (CFD), Engine air inlet, Air intake

ABSTRAKT

Tato studie využívá výpočetní dynamiku tekutin (CFD) k porovnání aerodynamického výkonu dvou odlišných návrhů nasávacích otvorů pro motorové závodní a sportovní vozy: jeden na způsob ponořeného nasávacího otvoru NACA a druhý jako střešní nasávací otvor. Tyto návrhy představují dva běžné přístupy v aerodynamice závodních vozů, každý se svými výhodami i nevýhodami. Pro motor je jedním z klíčových faktorů pro jeho výkon tlak, pod kterým je vzduch dodáván do spalovací komory, proto je důležité vstup navrhnout takovým způsobem, aby došlo k co možná nejnižším tlakovým ztrátám. Výsledky umožňují lépe pochopit, jak jednotlivé návrhy fungují, ty jsou následně porovnány a jsou navržena možná zlepšení a řešení pro další iterace.

KLÍČOVÁ SLOVA

Aerodynamika, Computational Fluid Dynamics (CFD), Vstup vzduchu do motoru, Přívod vzduchu

BIBLIOGRAPHIC CITATION

GALÁŠ, Jáchym. *Aerodynamic design of racing car engine air intake.* Brno, 2024. Available at: https://www.vut.cz/studenti/zav-prace/detail/157978. Bachelor's Thesis. Brno University of Technology, Faculty of Mechanical Engineering, Institute of Aerospace Engineering. Thesis supervisor Robert Popela.

DECLARATION

I declare that this thesis is my original work, which I have developed independently under the guidance of Ing. Robert Popela, Ph.D. using the literature and sources listed in
in the list attached to this thesis.

In Brno, 23rd May 2024 ……..…….

Jáchym Galáš

ACKNOWLEDGMENT

I would like to thank Ing. Robert Popela, Ph.D. and Ing. Štěpán Kaspar for their professional guidance, helpfulness and valuable advice they provided me during the preparation of this bachelor's thesis.

1. Introduction **10**
2. Theoretical Background **11**
2.1. Boundary Layer 11
2.2. Drag 11
2.2.1. Pressure Drag and Friction Drag 11
2.2.2. Induced Drag 11
2.2.3. Spillage Drag 12
2.3. Ram Air Effect 12
2.4. Effects of Pressure on Engine Performance 12
2.5. Total Pressure Recovery 12
3. Design of Geometries **14**
3.1. Overview of the Submerged Inlet 14
3.2. Overview of the Scoop Design 18
4. CFD **20**
4.1. Introduction to Computational Fluid Dynamics 20
4.2. Geometries 20
4.3. Domain and Boundary Conditions 21
4.4. Mesh 24
4.4.1. Surface Mesh 24
4.4.2. Prismatic Layers 24
4.4.3. Volume Mesh 24
4.5. Turbulence Modeling 25
4.5.1. Turbulence Model k-ε 25
4.5.2. Turbulence Model k-ω 25
5. Results **27**
6. Discussion **31**
7. Conclusion **32**
8. References **33**

1. Introduction

For modern high-performance cars, be they sports cars or race cars, aerodynamic efficiency is an important factor in the context of design, and utilizing every part of the vehicle is crucial in order to maximize the car's performance. This approach is also used when it comes to the IC (internal combustion) engine itself, as the components of the engine intake affect the combustion happening in the IC engine and therefore the power output.

The main objective of this study is to analyze and gain an insight into the working principles of two designs, each following a different design philosophy: a NACA-style submerged inlet and a roof scoop. Specifically, the goal is to evaluate the aerodynamic performance, airflow characteristics, and overall effectiveness of each intake design using CFD simulations by comparing these two designs under equal and steady conditions. The results yielded by CFD are then compared, and ideas for design optimization are proposed.

2. Theoretical Background

2.1. Boundary Layer

The boundary condition for a fluid in contact with a solid states that there is no "slip" between the fluid and the solid [4]. Combined with the fluid's viscosity, layers are created where the fluid's molecules move slower than the moving air.

Theoretical analyses of most aerodynamic flows treat the region away from the body as an inviscid flow (i.e., no dissipative effects due to friction, thermal conduction, or mass diffusion), and the thin region immediately adjacent to the body surface as a viscous flow where these dissipative effects are included. The thin viscous region adjacent to the body is called the boundary layer; for most aerodynamic problems of interest, the boundary layer is very thin compared to the extent of the rest of the flow. It is the source of the friction drag on an aerodynamic body. [5]

2.2. Drag

The drag force, often referred to simply as drag, is the net force exerted by a fluid on a body in the direction of flow due to the combined effects of wall shear and pressure forces. It is often instructive to separate the two effects, and study them separately. [4]

Drag is further normalized to the coefficient of drag by the equation

$$C_D = \frac{D}{\frac{1}{2} \cdot \rho \cdot v^2 \cdot A} \tag{1}$$

for which D is the drag force, ρ describes the fluid density, v stands for the flow velocity relative to the object with A being the reference area, in this case the vehicle's frontal area. [4]

2.2.1. Pressure Drag and Friction Drag

The part of drag that is due directly to wall shear stress tw is called the skin friction drag (or just friction drag FD, friction) since it is caused by frictional effects, and the part that is due directly to pressure P is called the pressure drag (also called the form drag because of its strong dependence on the form or shape of the body). The friction and pressure drag coefficients are defined below in equation (2). [4]

$$C_{D,friction} + C_{D,pressure} = C_D \tag{2}$$

2.2.2. Induced Drag

The pressure difference between high-pressure and low-pressure regions drives the fluid from the high-pressure area to the low-pressure area. Additionally, due to the relative motion between the fluid and the body, the fluid is swept toward the back. This results in a swirling motion that spirals along the flow, known as a vortex. [4]

Vortices interact with the free stream and impose forces on the edge in all directions, including the flow direction. The component of the force in the flow direction adds to the drag and is called induced drag. [4]

2.2.3. Spillage Drag

Spillage drag occurs when the air "spills" around the outside of the inlet instead of flowing into the engine. As the air spills over the external lip, it accelerates and the pressure decreases. This produces a lip suction effect that partially cancels out the drag due to spilling. [12]

2.3. Ram Air Effect

Both designs utilize the ram air effect, an aerodynamic phenomenon caused by the vehicle's forward motion, which forces air into a confined space. This increases the air pressure due to the limited volume and raises the air velocity due to the conservation of mass and energy. [4] [7]

The higher pressure created by the ram air effect allows a greater mass of air to enter the engine. This increased air mass flow rate can lead to more efficient combustion, potentially increasing the power output of the engine. [2]

2.4. Effects of Pressure on Engine Performance

The high amount of air increases the potentiality of fuel chemical elements to be burned with oxygen. As a result, engine performance and fuel economy are increased while simultaneously unburned exhaust emission components are reduced. Higher air intake pressure supplies more oxygen to combine with fuel elements in improving the combustion process. [15]

2.5. Total Pressure Recovery

Total pressure recovery is the difference of the free stream static pressure subtracted from the total pressure at the inlet's connection to the internal piping, divided by the free stream's dynamic pressure, as seen in equation (3). [7]

$$\xi = \frac{P_{tot} - P_{\infty}}{\frac{1}{2} \cdot \rho \cdot V_{\infty}^2} \tag{3}$$

where P_{tot} is the total pressure at the inlet's interconnection to the inner piping, P_{∞} describes the free stream absolute pressure, ρ is the density and V_{∞} represents the free stream velocity. In principle, if the flow moves through the inlet without any friction losses, this coefficient can reach its maximum value of 1.0. A higher pressure recovery indicates a better performing inlet. However, as the inlet speed V_i (an average speed at the inlet) reaches higher values, the friction losses increase due to the inner boundary layer and flow separations. [7]

Figure 1 shows that the submerged inlet is usually less efficient at the higher inlet flow rates, compared to the raised air scoop, because of the boundary layer ahead of the inlet. [7]

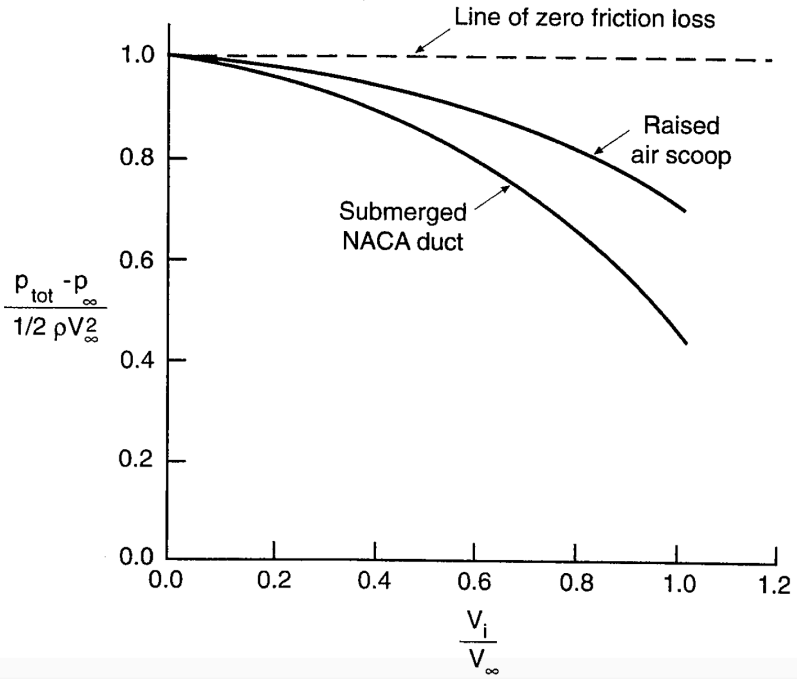

Figure 1 Total pressure recovery of typical inlets [7]

3. Design of Geometries

With the MR (engine in the middle, power to rear axle) configuration as one of the most popular design philosophies in both sports car and race car design due to its effect on the vehicle's handling in corners, the most common intake placement for mid-engine cars is on the roof. The IC engine in question is a naturally aspirated 5.2-liter 10-cylinder. Based on the 4-stroke thermodynamic cycle known as the Otto cycle, which has developed into one of the most widely used methods of power generation, especially for automobiles.

The key points regarding the design of an IC engine air intake are as follows:

- Total pressure recovery: To improve combustion efficiency, the shape of the inlet should efficiently recover the incoming air's total pressure, as it contributes to achieving higher pressure in the combustion chamber, thus supplying the engine with more oxygen. [7]
- Turbulence minimization (both inside and outside): Turbulent airflow can negatively affect the combustion within the IC engine, reducing its efficiency. [18]
- Drag reduction: Minimizing aerodynamic drag is essential to improving the overall efficiency and speed of a vehicle. Inlet designs must balance adequate airflow with low drag to prevent unnecessary resistance. [7]

3.1. Overview of the Submerged Inlet

The submerged inlet is to be designed in the style of a NACA duct. A NACA duct, often referred to as a NACA submerged inlet, is commonly used as an air intake duct. A submerged inlet allows air to enter the intake without interfering with the outside flow. [19]

Due to the fact that the submerged inlet does not extend outside of the vehicle's geometry, it is capable of achieving low aerodynamic drag and no requirements for specific structural reinforcements, causing no impact on the weight of the vehicle. Its operation is based on the combination of a diverging ramp and the profile of the sidewalls, which create counter-rotating vortices, deflecting the boundary layer away from the inlet and promoting potential flow. The boundary layers of interest in the submerged inlet are those developed on the ramp floor and the ramp walls. [3] [6]

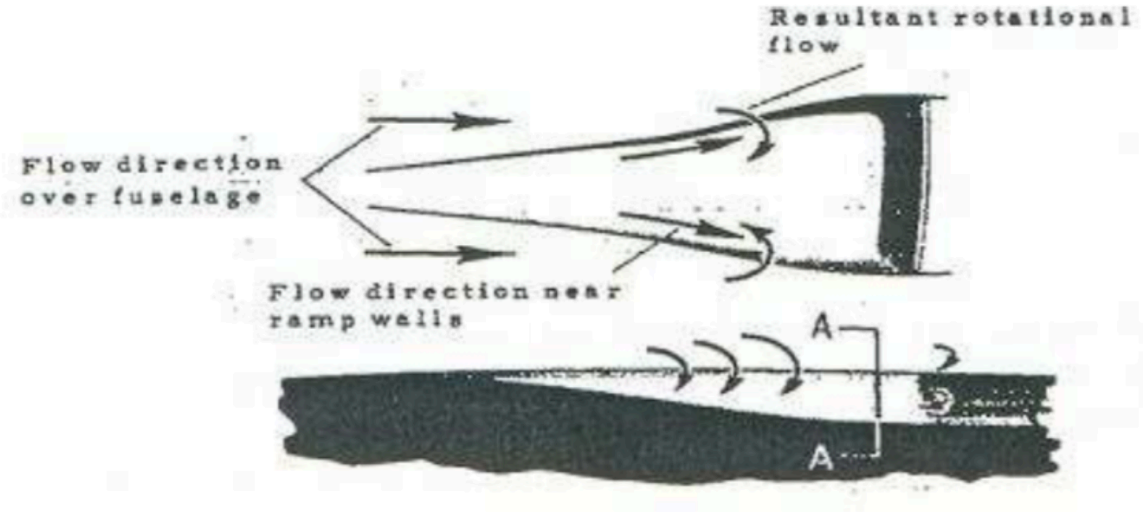

Figure 2 Flow structure of the NACA duct [9]

The external stream, depicted in Figure 2, not being parallel to the ramp walls, must flow over the top of the walls into the inlet. According to experimental analysis done by NACA, the best pressure recoveries were obtained with the curved divergence 4 which gave a maximum pressure recovery of 73 percent at an inlet velocity ratio of 0.40. Tests of the first divergent walls showed a surprising increase in the pressure recovery of to 10 percent at inlet velocity ratios less than 1.0. [1]

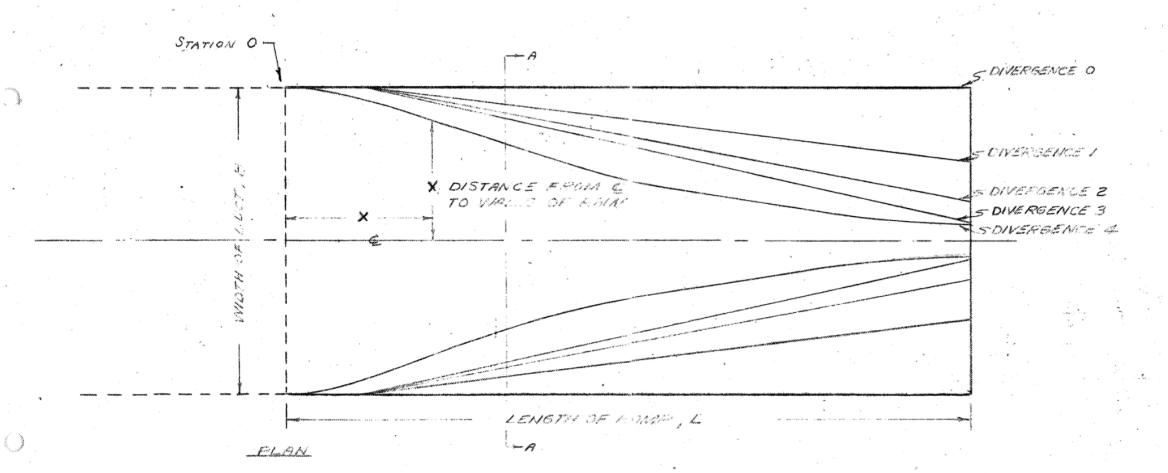

Figure 3 Types of ramp divergence of a NACA duct [1]

The results of NACA-conducted tests of various ramp angles with divergent walls presented in Figure 3 show the effectiveness of the divergence in increasing the ramp angle up to 10°. For 15° ramp angle, there is a significant loss in pressure recovery. It should be explained that the measure of divergence used in this investigation is the ratio of the width and the entrance of the ramp to the width of the submerged entrance. [1]

An example of a NACA submerged inlet implemented into a contoured surface is depicted in Figure 4 below. In this analysis, divergence 4 is used for the design with the ramp angle of 10°.

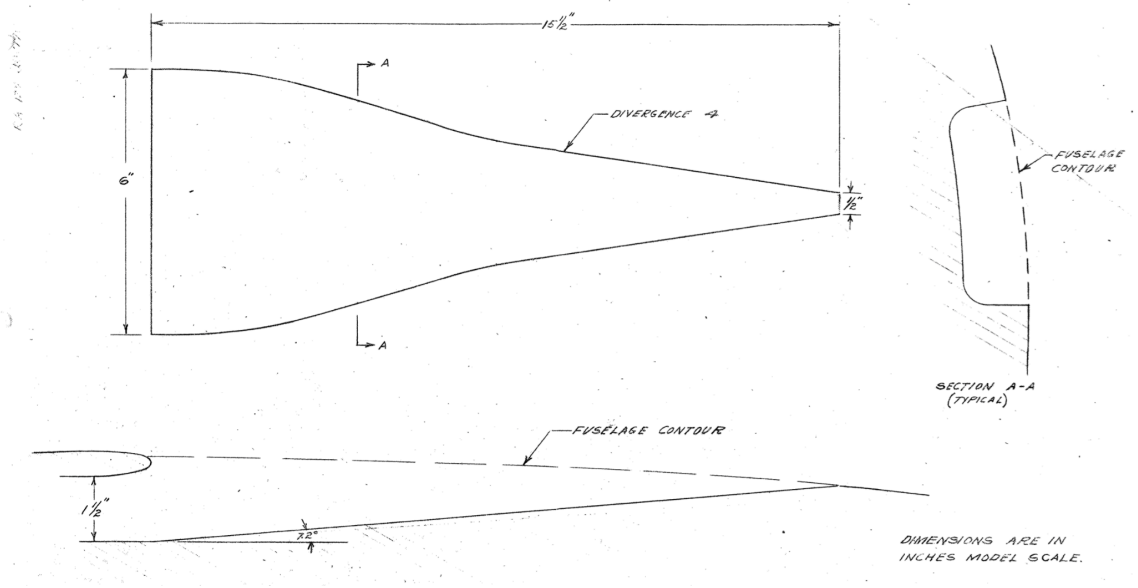

Figure 4 Sketch of a NACA submerged inlet in a contoured surface [1]

The CAD model of the NACA submerged inlet can be seen in Figure 5.

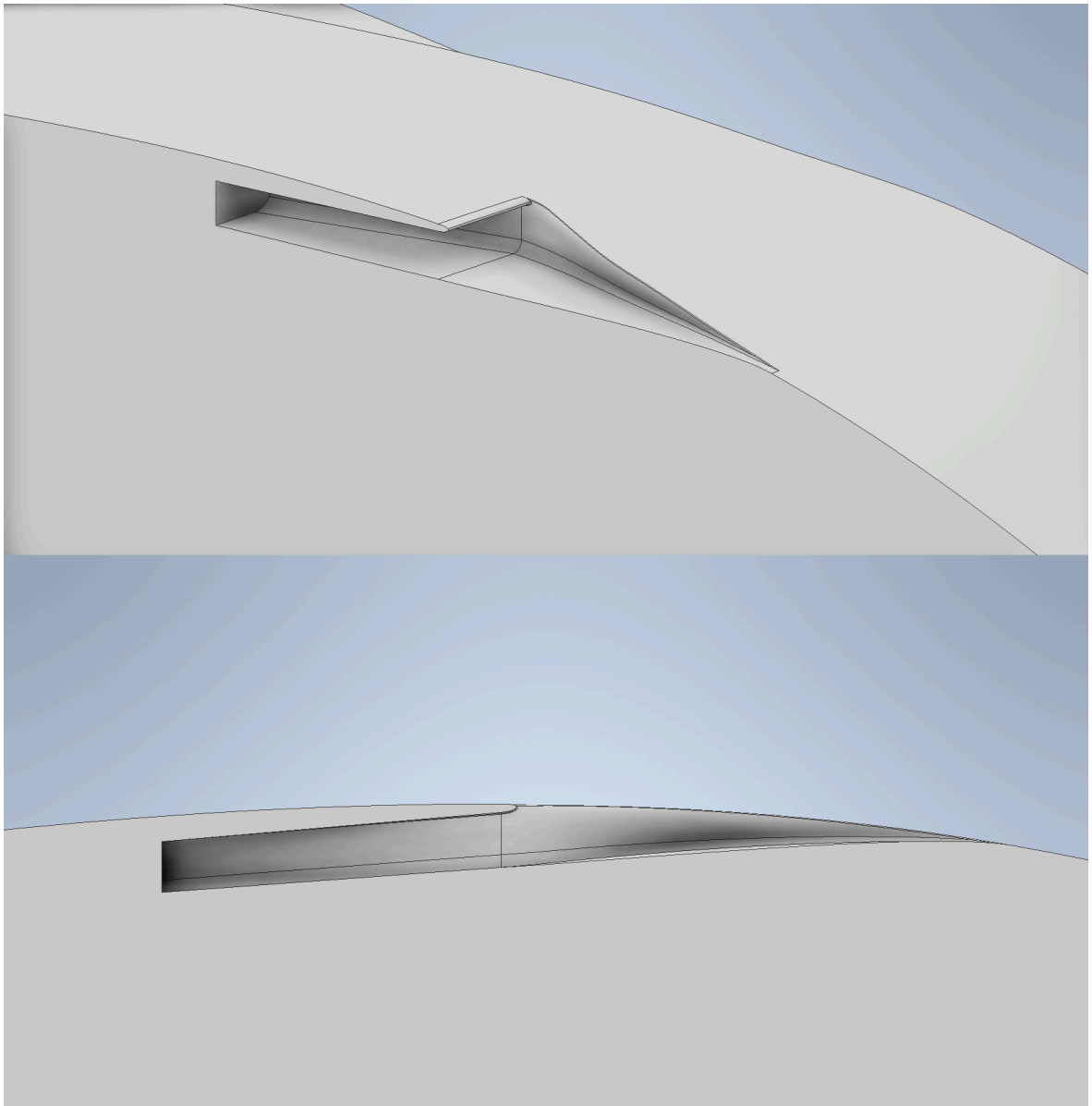

Figure 5 Detail view of the submerged inlet design positioned on the vehicle's roof (top) and the section view from symmetry plane (bottom)

3.2. Overview of the Scoop Design

With its roots in rally and endurance racing, the roof scoop channels clean, high-velocity airflow into the engine. The elevated position of roof scoops helps in drawing cleaner air compared to lower-placed intakes, thus ensuring a more consistent and efficient supply of air to the engine, as seen in Figure 6. [7]

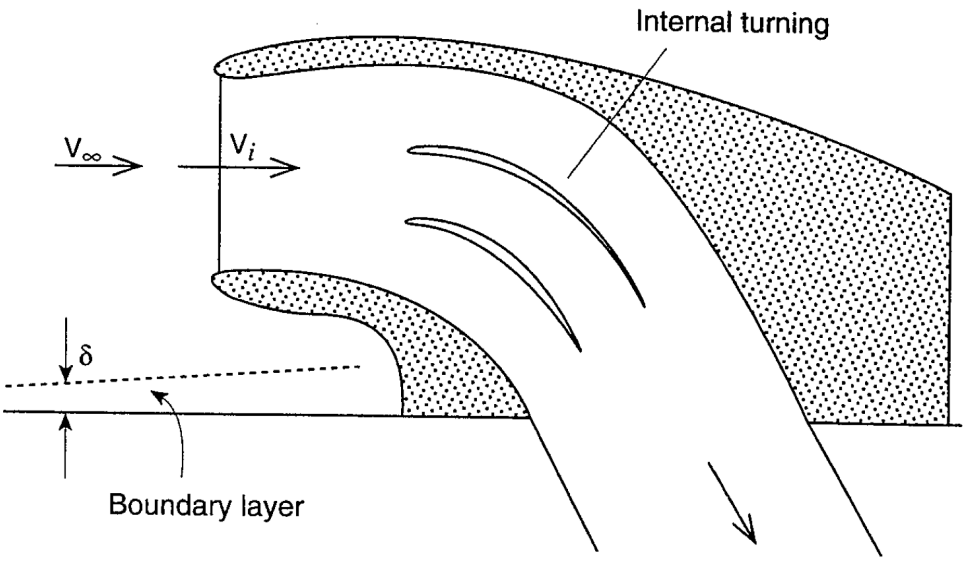

Figure 6 Typical raised inlet [7]

For more effective operation, the scoop is to be mounted in areas of the vehicle where the boundary layer is thin [7] [13]. Figure 7 shows the designed inlet.

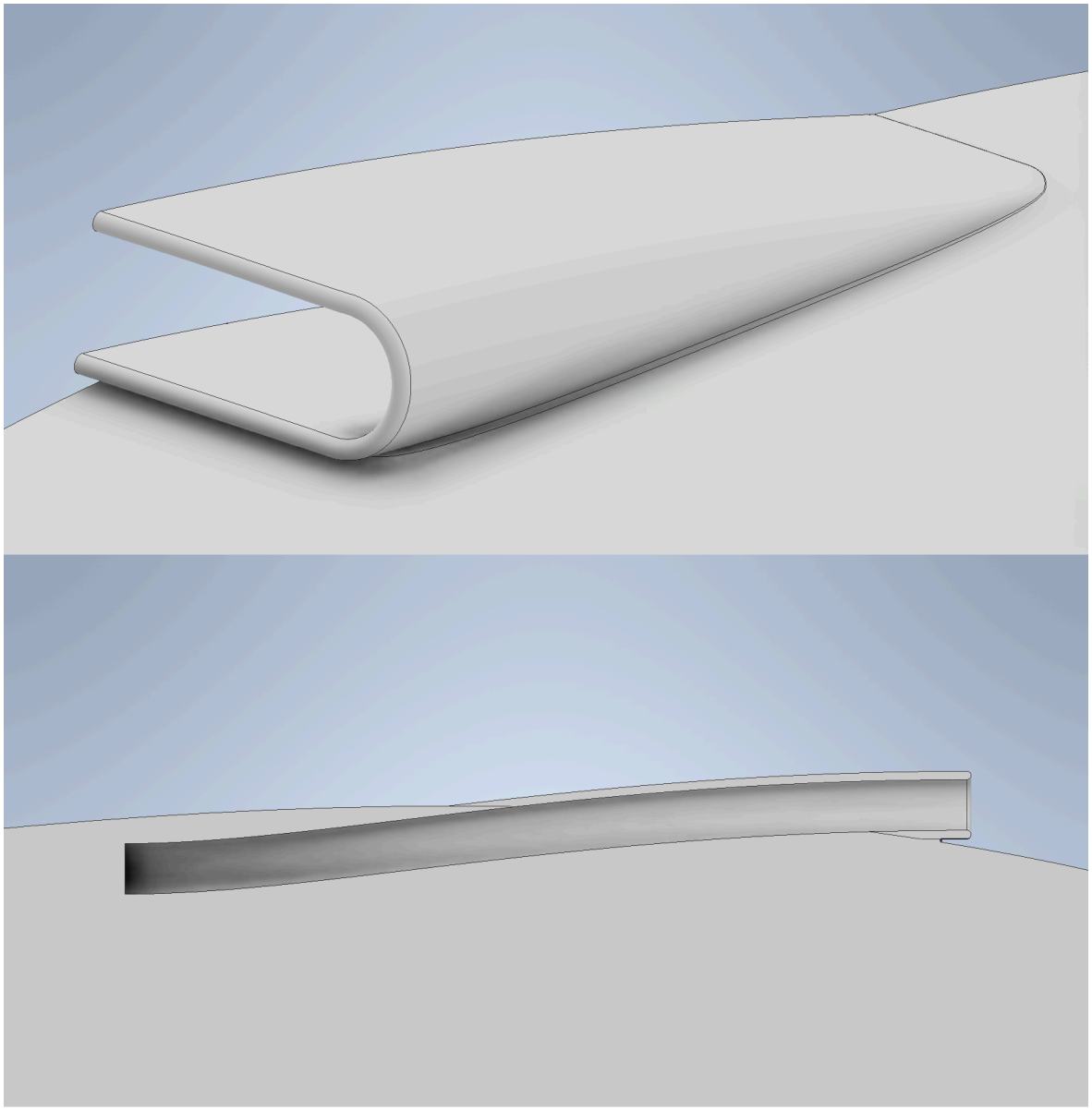

Figure 7 Detail view of the roof scoop inlet (top) and its section view from the symmetry plane (bottom)

4. CFD

4.1. Introduction to Computational Fluid Dynamics

Computational Fluid Dynamics (CFD) revolves around the numerical simulation and analysis of fluid flow and heat transfer using the finite element method. It enables engineers to study and estimate the behavior of fluids when dealing with complex geometries and scenarios. The main principle of CFD involves discretizing the main equations of fluid flow, the Navier-Stokes equations, into a set of algebraic equations that can be solved numerically.

The analysis of fluid flow can nowadays be done with high effectiveness and accuracy thanks to CFD. Through the simulation of airflow patterns, pressure distributions, and aerodynamic properties, CFD allows engineers to analyze their designs. In comparison with wind tunnels, CFD analysis is much more affordable, which is why it is widely used in any engineering field that deals with fluid flow. In this study, Ansys Fluent is used to carry out the computations.

4.2. Geometries

In order to save computational power and therefore time for calculating, geometry is to be cut in half along the plane of symmetry and simplified in areas that do not have any significant effect on the investigated inlet, such as the car's underbody. Following this approach, the underbody can be deemed unnecessary to study, and thus it is possible for it to be simplified. The simplified model can be seen in Figure 8.

Both designs have to follow the given parameters, which state that both must have the same inlet area and the same cross section at the inlet's interconnection to the internal piping. The software that is used to model the simplified model of the vehicle is Autodesk Inventor.

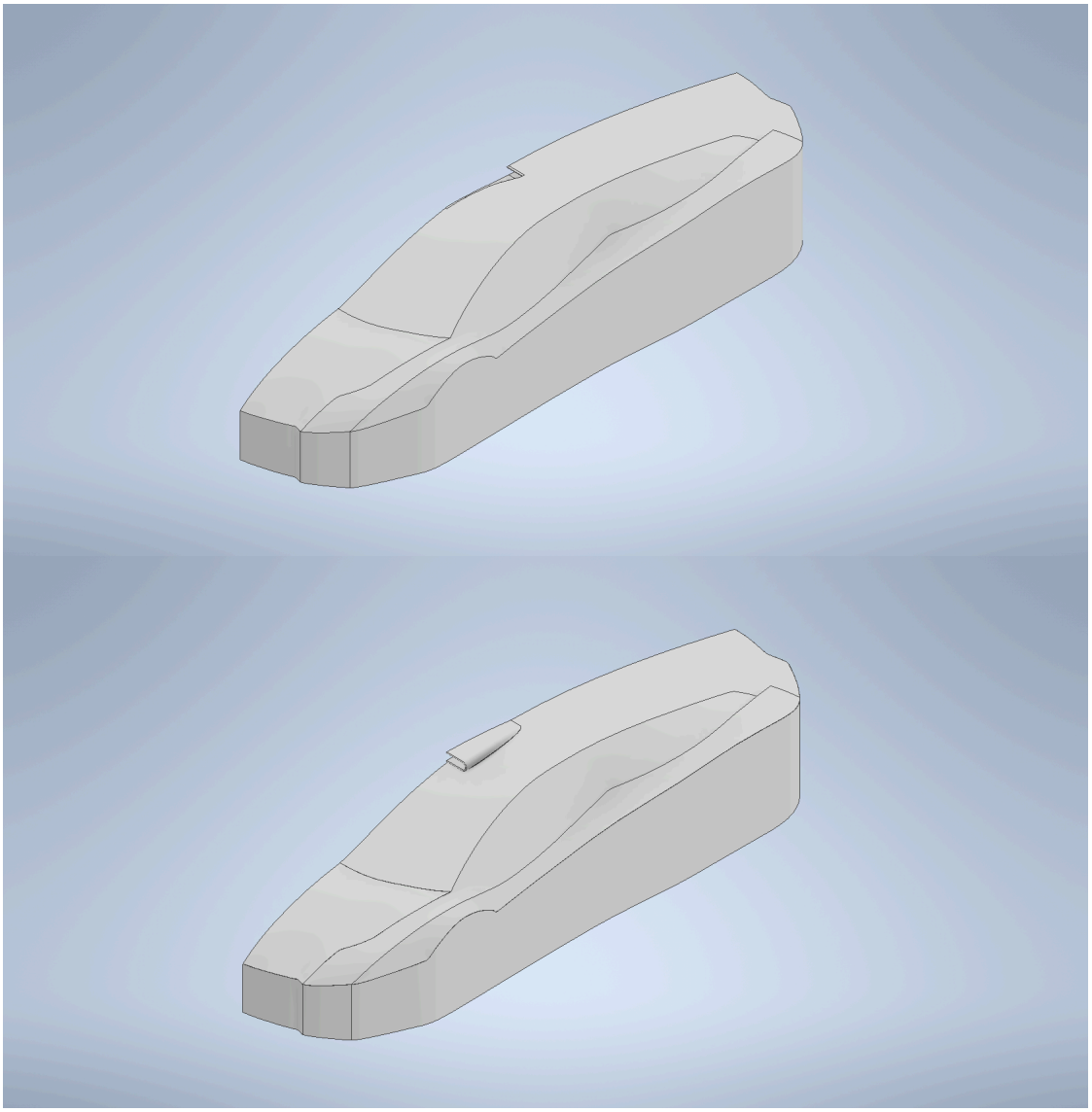

Figure 8 Simplified vehicle geometries - submerged inlet (top), roof scoop (bottom)

4.3. Domain and Boundary Conditions

The domain refers to a region within which the fluid (air in this case) is simulated. It should be large enough to capture all relevant flow features but not excessively because with the increase of the domain size the computational costs also grow. The size of the domain is 5 car lengths forward, 10 backward, 3 upward and 3 sideways with respect to the location of the vehicle's geometry.

Boundary conditions used in the simulation:

- Velocity inlet
- Pressure outlet
- Mass flow outlet
- No-slip wall
- Slip wall
- Symmetry

The velocity inlet is set to 60 m/s as the uniform velocity of the incoming air, traveling through the car and exiting through the plane, with the pressure outlet BC set to standard atmospheric pressure behind the vehicle. The comparison of the two inlets is done with the assumption of an equal mass flow of air for both. The mass flow outlet BC is calculated by the following equations for the calculation of engine air demand multiplied by the density of air at 15°C with the engine running at 6000 rpm at 0.85 volumetric efficiency.

$$\dot{V} = \frac{1}{2} \cdot V_{cylinder} \cdot \frac{n}{60} \cdot \eta \tag{4}$$

$$\dot{m} = \rho \cdot \dot{V} \tag{5}$$

For simplification and to save computational power, the slip-wall BC is used on the ground to avoid the need to generate additional prismatic layers. The solid objects are set as no-slip walls. As already mentioned in 4.1, the last boundary condition, which allows to save computational power and therefore time needed for computations, is the symmetry BC, which is used on the symmetry plane of the car. The BC layout can be viewed in Figure 9.

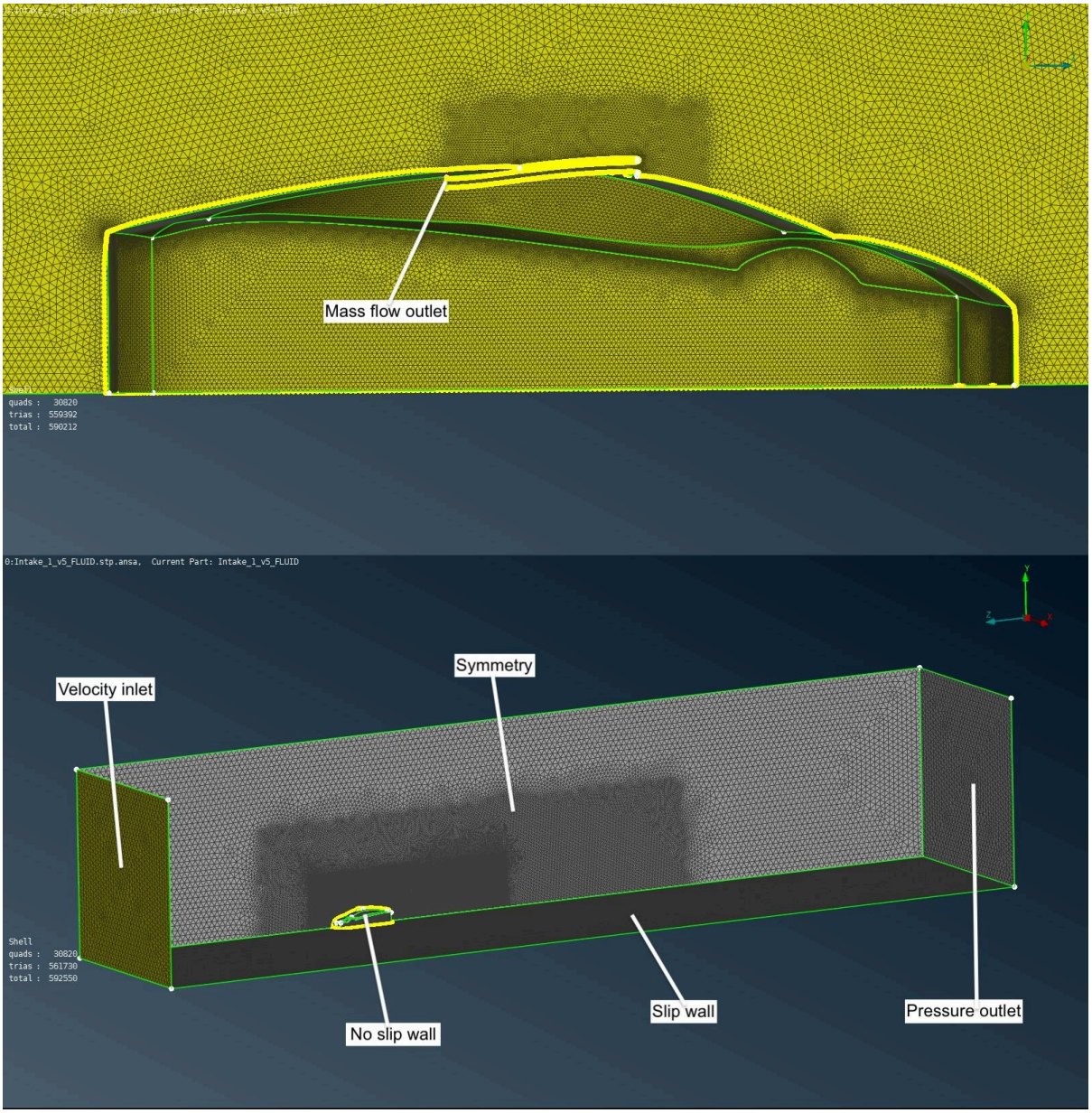

Figure 9 Domain and boundary conditions

4.4. Mesh

The BETA CAE Systems ANSA pre-processor is used to generate the computational mesh. As in any other case where the finite element method is used, the construction of a computational mesh is required. Such a mesh consists of separate elements (or cells) into which the whole domain is divided. Generally, with smaller cells, the accuracy rises; however, this comes with the cost of computational power and therefore the time needed for the computer to yield a result.

In order to balance the computational power (time) and accuracy, the mesh is usually fine in the proximity of the investigated geometry. In areas further from said geometry, where the flow of the fluid is more uniform, the size of the cells can increase for faster calculations.

4.4.1. Surface Mesh

The initial step in the mesh creation process is the surface mesh. This is the main factor that determines the size and, therefore, the quality of the cells.

In CFD, the quality of the surface mesh is greatly affected by any sharp edges present in the geometry. For this reason, sharp edges need to be rounded. These rounded edges, even though they may not be the main focus of the analysis, require a small element size for the cells not to deform.

4.4.2. Prismatic Layers

The boundary layer present on the walls' surface needs its own mesh in order to be accurately calculated. This mesh is constructed using the so-called prismatic layers, which are described by the dimensionless quantity y^+ seen in equation (3).

$$y^+ = \frac{y \cdot u_* \cdot \rho}{\mu} \tag{3}$$

where y is the boundary layer height, u* is the shear velocity, ρ is the air density, and μ stands for the kinematic viscosity. [14]

4.4.3. Volume Mesh

Three-dimensional cells are dependent on the surface mesh, on whose surface the prismatic layers are generated. The volume mesh type used in practice for vehicles is the HexaPoly seen below in Figure 10.

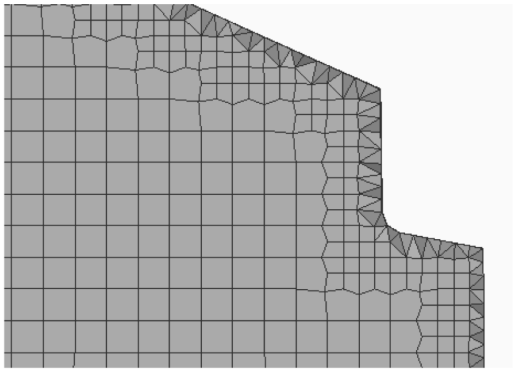

Figure 10 HexaPoly volume mesh [10]

This type combines variable-size hexa- and polyhedral elements inside the domain with transitions of polyhedrons and tetrahedrons near the surface. When far enough from the surface, cubic cells are generated instead. [10]

4.5. Turbulence Modeling

Turbulent flow is governed by the Navier-Stokes momentum equations, the continuity equation, and, in compressible flow, energy and state equations. There are multiple ways to model turbulence in computational fluid dynamics, with the Direct Numerical Simulation (DNS) being the most accurate one where the Navier-Stokes equations are solved directly. However, the drawback here is that the demand in terms of computational power is too large, and thus the DNS is rarely used. The least demanding method in terms of computational power and therefore time is the RANS (Reynolds Averaged Navier Stokes) method, which uses time-averaged values to solve the simulation as a steady-state case. [11]

4.5.1. Turbulence Model k-ε

The standard k-ε model is based on model transport equations for two quantities: turbulence kinetic energy (k) and turbulent dissipation rate (ε). The model transport equation for k-ε is derived from the exact equation, while the model transport equation for k-ε is obtained using physical reasoning and bears little resemblance to its mathematically exact counterpart. [16]

The k-ε model typically requires wall functions to resolve turbulence near walls, as it has difficulties accurately capturing how the flow behaves close to the wall. [8]

4.5.2. Turbulence Model k-ω

In describing turbulence, many researchers refer to eddying motion, which is a local swirling motion where the vorticity can often be very intense. The turbulence model k-ω is used in this analysis, which is another two-equation turbulence model with the quantity ω referred to as the rate of dissipation of turbulent kinetic energy per unit turbulent kinetic energy and time, or also often described as specific turbulent dissipation rate. [8]

In contrast to the k-ε model, the k-ω includes a near-wall treatment that makes it more accurate in the near-wall region, allowing it to directly resolve the flow behavior down to the wall without the need for wall functions. [16] [17]

The most commonly used variation of SST (Shear Stress Transport) This hybrid model combines the strengths of both k-ω (near-wall treatment) and k-ϵ (free-stream performance) models, making it suitable for flows with adverse pressure gradients, separation, and complex boundary layers. [16] [17] [8]

5. Results

Both designs gave similar results in terms of average pressure losses and total pressure recovery coefficient. Results differ significantly in the car's total drag coefficient. The mean (average) value of the total pressure losses ΔP_{loss} is explained in equation (6) as a difference of the total pressure measured over the mass flow outlet's cross section $P_{tot,AVG}$ and the free stream total pressure $P_{\infty tot}$ can be seen in Table 1 along with the total pressure recovery coefficient ξ, calculated by equation (3), and the total drag coefficient of the car $C_{D,car}$.

$$\Delta P_{total} = P_{tot,AVG} - P_{\infty tot} \tag{6}$$

Table 1 also shows a direct comparison in the form of percentage differences between the two inlets in order to better represent how much each design differs from the other. This percentage difference is calculated as per equations (7), (8), and (9), with each index denoting its corresponding inlet.

$$\Delta P_{total}\ Percentage\ Difference = \frac{\Delta P_{total,scoop} - \Delta P_{total,submerged}}{\Delta P_{total,submerged}} \cdot 100 \tag{7}$$

$$\xi\ Percentage\ Difference = \frac{\xi_{scoop} - \xi_{submerged}}{\xi_{submerged}} \cdot 100 \tag{8}$$

$$C_{D,car}\ Percentage\ Difference = \frac{C_{D,scoop} - C_{D,submerged}}{C_{D,submerged}} \cdot 100 \tag{9}$$

Table 1 Resulting values

	Avg. Pressure Losses	Total Pressure Recovery Coeff.	Total Car Drag Coeff.
Metric	ΔP_{loss}	ξ	$C_{D,car}$
Submerged Inlet	-419.990 [Pa]	0.8096 [-]	0.1522 [-]
Roof Scoop	-462.844 [Pa]	0.7901 [-]	0.1789 [-]
Percentage diff. (scoop vs. submerged)	10.204 [%]	-2.409 [%]	17.543 [%]

Using ANSYS EnSight, it is possible to create useful images representing the behavior of computed quantities achieved by the solver. The total pressure losses represented by the cold colors occurring over the cross section of the inlet's interconnection to the inner tubing can be viewed in Figure 11, where the average total pressure losses ΔP_{total} are referred to as delta_P_total.

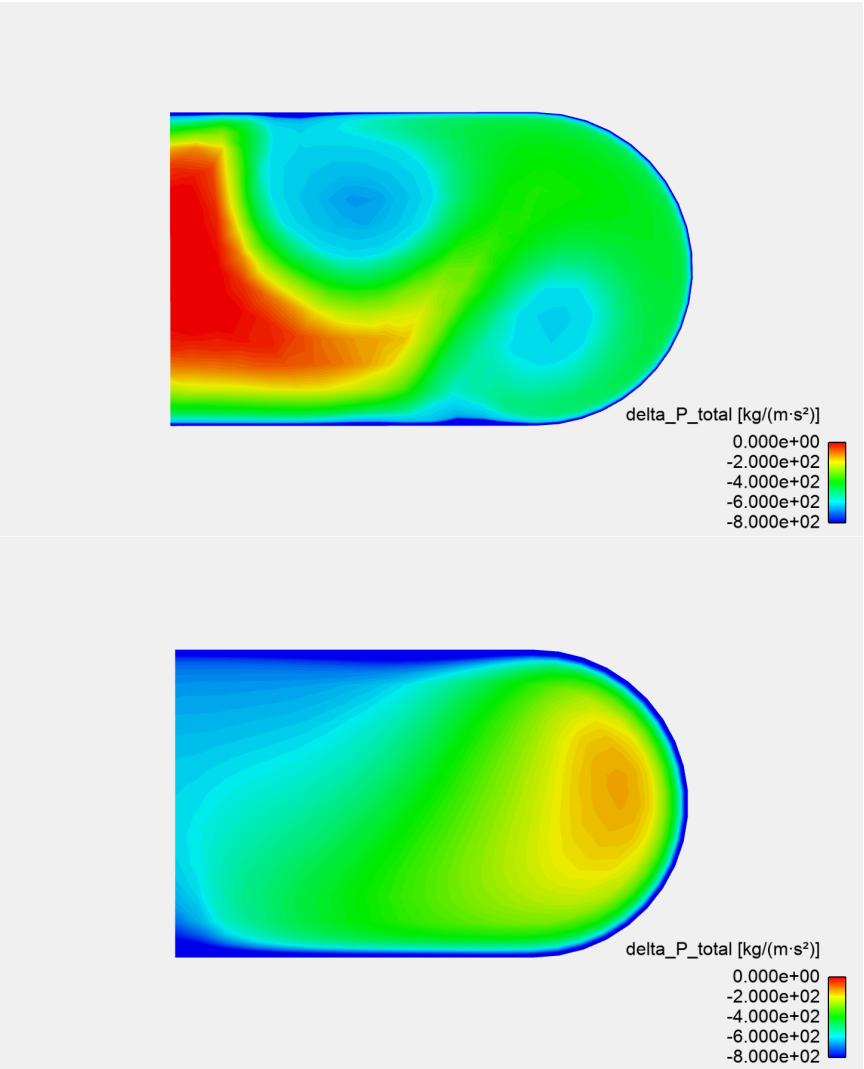

Figure 11 Total pressure distribution over the inlet exit cross section: submerged (top), air scoop (bottom)

For the submerged inlet, the results indicate that an additional vortex formed along the path, causing a non-uniform distribution. As for the roof scoop inlet, total pressure is highest on the sides, also showing non-uniformity in distribution.

Figure 12 describes the velocity profile on the symmetry plane of the geometry. The submerged inlet's total pressure distribution is uniform over the symmetry plane, according to

the computations, and does not undergo any noticeable pressure losses. In contrast, the roof scoop appears to be affected by a vortex forming near the bottom lip due to accumulation of air.

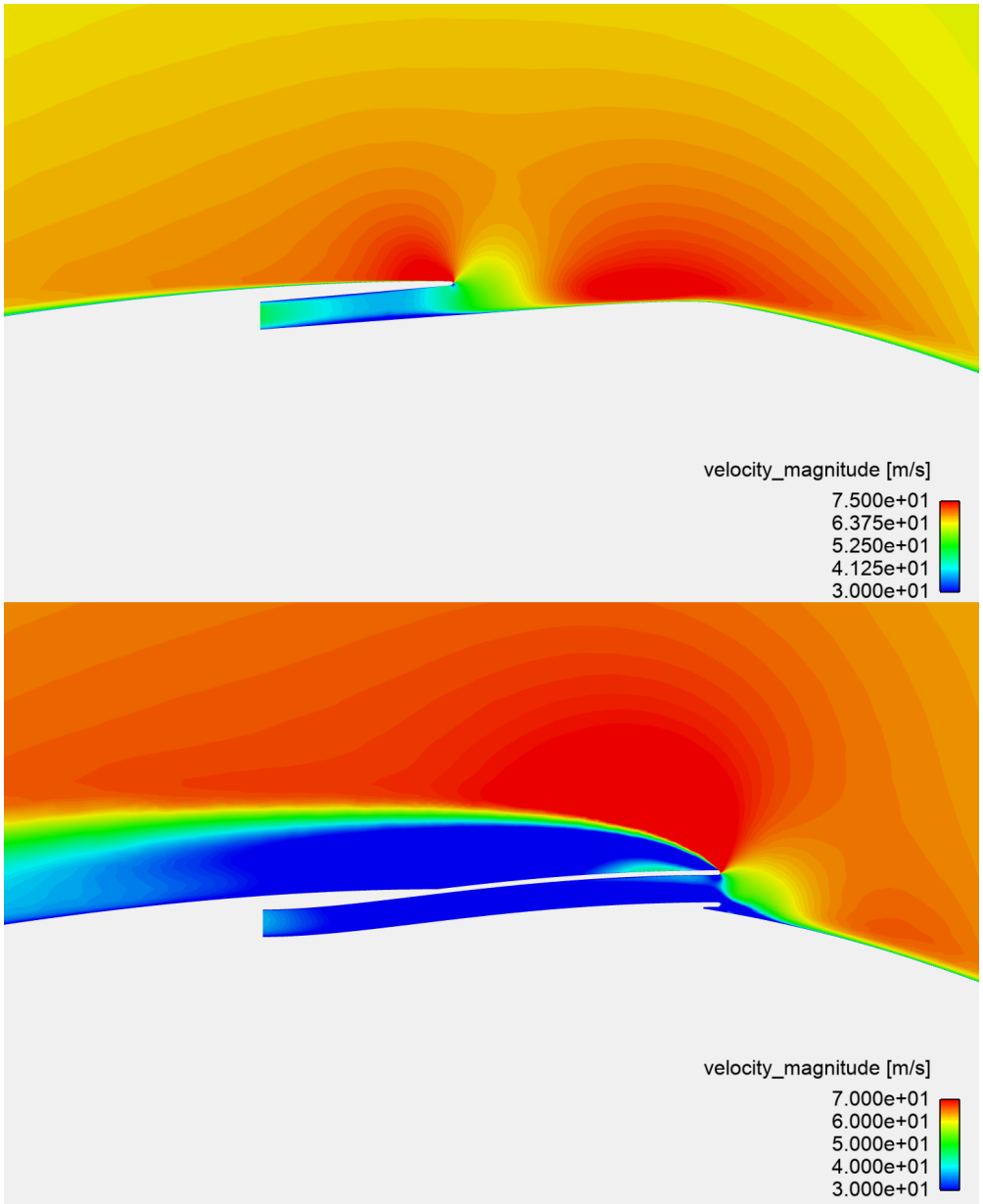

Figure 12 Velocity profile on the symmetry plane: submerged (top), air scoop (bottom)

Another noticeable issue would be the flow separation occurring on top of the scoop, which hints at the fact that the angle of attack of the inlet with respect to flow direction is too high.

Figure 13 describes the airflow's behavior as it travels through the inlet. The aforementioned additional vortex starts forming approximately in the same spot where the inlet starts converging into the inner piping.

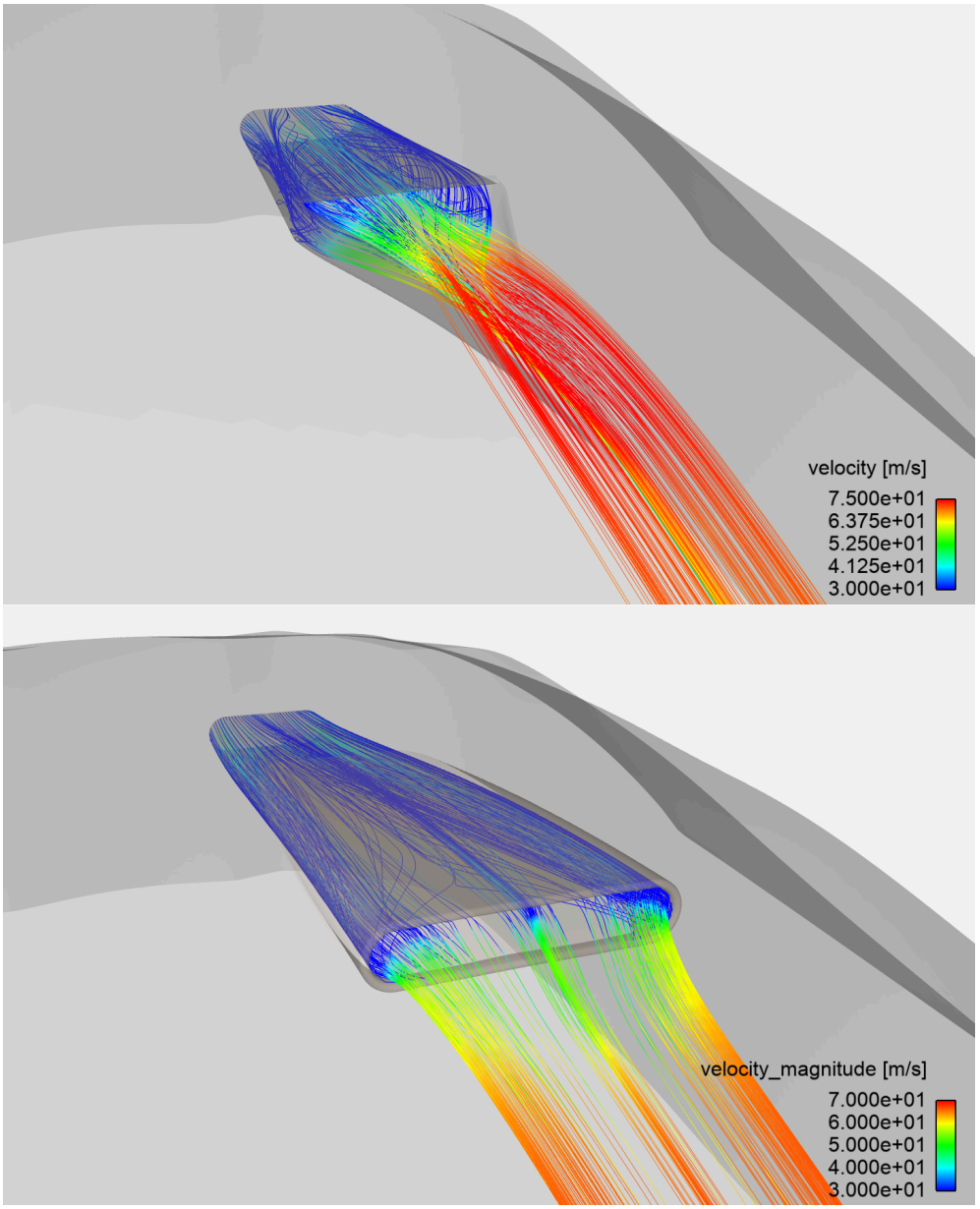

Figure 13 Streamlines colored by velocity magnitude flowing through the inlet - submerged (top), air scoop (bottom)

6. Discussion

The CFD simulations show that the submerged inlet is capable of achieving high pressure recovery with the boundary layer not separating on the divergent ramp. A high-velocity region above the lip is present, although without flow separation. The unexpected vortex formation affects the airflow by introducing unwanted turbulence, which would negatively affect engine performance. Prolonging the converging part of the intake or downsizing the opening are recommended to allow for a smoother transition, potentially preventing the additional vortex formation.

The simulations of the roof scoop yield similar results in terms of pressure recovery, being marginally less efficient. The drag coefficient is higher, partially due to the scoop's increase in the car's frontal area. Another factor contributing to the increase in drag is the separation happening on top. Inside the air scoop, the airflow is more uniform as no vortices are formed. However, the air gathers below the lower lip, forming a small vortex. This could be improved by implementing a diverter to the scoop's underbody. The separation happens due to the angle of attack in relation to the incoming stream, which would need to be countered by either repositioning the inlet further back, preferably to the apex of the car, or by modifying the geometry so that it is parallel to the streamlines.

7. Conclusion

The goal of this study is to analyze and compare two engine air intake designs using CFD to gain an understanding and insight into the functioning principles of each one. Initially, a search is conducted for the theoretical background and design guidelines of each engine air inlet. Then a model of a vehicle based on the idea that every aspect of the vehicle's geometry except the airflow path leading to the intake is simplified. Subsequently, a computational mesh is generated and further set up with the necessary boundary conditions. After computing, post-processing is carried out in order to comprehensively interpret the results obtained.

Two designs that go in opposite directions in terms of design philosophy have yielded comparable results, which provided insight into their working principles; thus, the goal of this study is completed. Despite the superior performance of the submerged inlet in the analysis, manufacturers tend to prefer the roof scoop design in practical applications. In reality, the mass flow the roof scoop is capable of could outperform the submerged inlet, as it is located above the turbulent boundary layer.

It is essential to consider potential numerical errors that could impact the determination of the superior design. For a more comprehensive and precise analysis, a more accurate geometry, inclusion of all relevant factors and a refined computational mesh would be necessary to obtain more accurate results.

8. References

[1] FRICK, Charles W. et al. *An experimental investigation of NACA submerged-duct entrances* [online]. 1945. Available at: https://ntrs.nasa.gov/citations/20090012113

[2] CONSTANDI, J. S. *Air Induction Design for Restricted Race Engines*. Online. https://core.ac.uk/download/pdf/37749992.pdf.

[3] ALMEIDA, Odenir de; Pedro Correa SOUZA; Erick CUNHA. *A numerical approach for implementing air intakes in a canard type aircraft for engine cooling purposes* [online]. Journal of Aerospace Technology and Management, 2021, 13: e0221.

[4] ÇENGEL, Yunus A. and John M. CIMBALA. *Fluid Mechanics: Fundamentals And Applications*. Tata McGraw Hill Education Private Limited, 2010.

[5] ANDERSON, John. F*undamentals of Aerodynamics*, 6th Edition, Tata McGraw Hill Education Private Limited.

[6] SACKS, Alvin H. and John R. SPREITER, *Theoretical investigation of submerged inlets at low speeds* [online]. 1951. Available at: https://ntrs.nasa.gov/citations/19890067876

[7] KATZ, Joseph. *Race car aerodynamics: designing for speed*. Revised 2nd edition.

Cambridge]: Bentley Publishers.com. 2006. ISBN 0-8376-0142-8

[8] WILCOX, David C. et al. *Turbulence modelling for CFD*. La Canada, CA: DCW industries. 1998.

[9] DELANY, Noel K., *An Investigation of Submerged Air Inlets on a 1/4-Scale Model of a Typical Fighter-Type Airplane.* 1948.

[10] BETA CAE SYSTEMS S.A. *ANSA for CFD Brief User Guide*

[11] LESCHZINER, Michael. *Statistical turbulence modelling for fluid dynamics - demystified: an introductory text for graduate engineering students.* London: Imperial College Press, 2015. ISBN 978-1-78326-661-6.

[12] HALL, Nancy. *Inlet Performance* [online]. National Aeronautics And Space Administration. 2021. Available at: https://www.grc.nasa.gov/www/k-12/airplane/inleth.html

[13] RÜTTEN, Markus; Lars KRENKEL; Malte FREUND. *Parametric design, comparison and evaluation of air intake types for bleedless aircraft*. In: 39th AIAA Fluid Dynamics Conference. 2009. p. 3902.

[14] *Y+ calculator. In: Omnicalculator* [online]. Available at: https://www.omnicalculator.com/physics/yplus

[15] ABDULLAH, Nik Rosli et al. *Effects of air intake pressure on the engine performance, fuel economy and exhaust emissions of a small gasoline engine* [online]. Journal of Mechanical Engineering and Sciences. 2014.

[16] ANSYS Inc. *Ansys Fluent Theory Guide.* 2021.

[17] MENTER, F. R. *Two-Equation Eddy-Viscosity Turbulence Models for Engineering Applications*. AIAA Journal, 1994

[18] HUCHO, W. *Aerodynamics of Road Vehicles: From Fluid Mechanics to Vehicle Engineering*. Butterworth-Heinemann. ISBN 0768000297

[19] ALTAIR ENGINEERING Inc. Naca Scoop Element [online]. 2021. Available at: https://2021.help.altair.com/2021.1/Naca_Scoop_Element.htm

9. Abbreviations

C_D	Coefficient of drag	[-]
$C_{D,friction}$	Coefficient of friction drag	[-]
$C_{D,pressure}$	Coefficient of pressure drag	[-]
$C_{D,car}$	Coefficient of drag of the vehicle	[-]
D	Drag Force	[N]
v	Velocity	[m/s]
ρ	Density	[kg/m^2]
A	Frontal area	[m^2]
ξ	Pressure recovery coefficient	[-]
P	Pressure	[Pa]
P_{tot}	Inlet total pressure	[Pa]
$P_{tot,AVG}$	Average inlet total pressure	[Pa]
$P_{\infty tot}$	Free stream total pressure	[Pa]
P_{∞}	Free stream absolute pressure	[Pa]
ΔP_{total}	Average total pressure loss	[Pa]
V_{∞}	Free stream velocity	[m/s]
y^+	Dimensionless wall distance	[-]
y	Wall distance	[m]
μ	Dynamic viscosity	[P*s]
u_*	Shear velocity	[m/s]
V	Engine cylinder volume	[m^3]
$\dot{V}$	Volume flow rate	[m^3/s]
n	Number of revolutions	[1/min]
η	Volumetric efficiency	[-]
$\dot{m}$	Mass flow rate	[kg/s]

IC	Internal Combustion
NACA	National Advisory Committee for Aeronautics
CFD	Computational Fluid Dynamics
RANS	Reynolds Averaged Navier Stokes
DNS	Direct Numerical Solution
BC	Boundary Conditions